Marine Pollution Bulletin 142 (2019) 43–53

Contents lists available at ScienceDirect

Marine Pollution Bulletin

journal homepage: www.elsevier.com/locate/marpolbul

Baseline

Radioactive level of coral reefs in the South China Sea

Wuhui Lin[a,b], Kefu Yu[a,b,*], Yinghui Wang[a,b,*], Xinming Liu[c], Qiuyun Ning[c], Xueyong Huang[a,b]

[a] Coral Reef Research Center of China, School of Marine Sciences, Guangxi University, Nanning 530004, China
[b] Guangxi Laboratory on the Study of Coral Reefs in the South China Sea, Nanning 530004, China
[c] Guangxi Academy of Oceanography, Nanning 530022, China

ARTICLE INFO

Keywords:
Coral reefs
Radioactivity
Sediment
$^{226}Ra/^{238}U$
Nuclear weapons testing

ABSTRACT

In this study, we examined radioactivity simultaneously in surface marine sediments and coral skeletons collected from 12 locations of the fringing and atoll reefs in the South China Sea. Radioactive level declined from the fringing reefs to atoll reefs because of input of terrigenous minerals in the fringing reefs. Radioactivity was higher in coral skeletons than in marine sediments because of the high ^{228}Ra activity in coral skeletons. Additionally, an abnormally low $^{226}Ra/^{238}U$ activity ratio (< 0.1) of marine sediments in coral reefs was attributed to the biological process of active uptake of ^{226}Ra and ^{238}U from seawater by coral polyps rather than the ingrowth process in the ^{238}U-^{230}Th-^{226}Ra decay chain. Several radiological indices were evaluated in coral reefs and significantly lower than recommended values. Particularly, the average Ra_{eq} in the atoll reefs was < 5% of the world's average of Ra_{eq}. Our results displayed typically radioactive status in coral reefs without close-in fallout of anthropogenic radionuclides.

Radionuclides are hazardous substances that may impose radiological risk to humans and biota (Johansen et al., 2015; W. Lin et al., 2015; W.H. Lin et al., 2015). Artificial radionuclides were dispersed globally and were recognized as a significant proxy for the "Anthropocene epoch" and biogeochemical processes (Hong et al., 2011; Waters et al., 2016). Therefore, the activity of radionuclides in the marine environment is widely measured and internationally compiled from the perspectives of environmental safety, human health, and scientific research (IAEA, 2005; UNSCEAR, 2000).

Coral reefs, as one of the typical marine ecosystems, are "hotspots" of high biodiversity and provide rich biological resources and significant tourist sites for humans (Moberg and Folke, 1999). The 2002 World Summit on Sustainable Development indicated that millions of people depend on coral reefs for their daily living. The radionuclides in coral reef fishes, the total species of which is > 5000 (Hixon and Randall, 2018), may impose ionizing radiation on humans through seafood consumption. The external radiation of radionuclides occurs during increasing human activity of SCUBA diving in coral reefs. The reef rock is also used for house construction by humans inhabiting on the coral islands. Overall, ionizing radiation exposure to humans takes place through all the above-mentioned exposure pathways in coral reefs. However, we still have very limited information about the radioactive status in coral reefs relative to many other environmental matrixes, such as crust (Van Schmus, 1995), rocks (Ojovan and Lee, 2014), sandy beach (Huang et al., 2015), soil (Liu and Lin, 2018), building materials (Trevisi et al., 2012), atmosphere (W. Lin et al., 2015), seawater (Lin et al., 2016a), and marine organisms (Stewart et al., 2008).

In the present study, radioactivity in surface marine sediments and living coral skeletons was simultaneously measured by high purity germanium (HPGe) γ-spectrometry in 12 locations of the fringing and atoll reefs in the South China Sea (SCS), which is adjacent to the Coral Triangle with the world's highest biodiversity (Veron et al., 2011). The SCS is the largest marginal sea of the North Pacific Ocean. These stations cover a latitude of 14° (> 1500 km). The behaviors of naturally occurring radionuclides (^{238}U, ^{226}Ra, ^{228}Ra, and ^{40}K) in the coral skeleton and marine sediment were also analyzed in this study. The radiological parameters including radium equivalent activity (Ra_{eq}), external and internal hazard indices (H_{ex} and H_{in}), representative gamma level index ($I_{\gamma r}$), absorbed gamma dose rate (D_R), and annual effective dose equivalent (AEDE) were also calculated to assess radiological hazards in coral reefs. We believe that our results will fill the gap in information about radioactive status in coral reefs located in the SCS and provide reference for the natural radioactivity before nuclear weapons testing in the Marshall Islands, whose physical settings are similar to those of our stations in the atoll reefs.

Naturally occurring radionuclides were simultaneously analyzed in marine sediments (top layer, within 2 cm from the surface) and living

* Corresponding authors at: Office 1111#, Zonghe Shiyan Building, Guangxi University, Nanning City, Guangxi Province, China.
E-mail addresses: kefuyu@scsio.ac.cn (K. Yu), wyh@gxu.edu.cn (Y. Wang).

https://doi.org/10.1016/j.marpolbul.2019.03.030
Received 25 November 2018; Received in revised form 6 March 2019; Accepted 13 March 2019

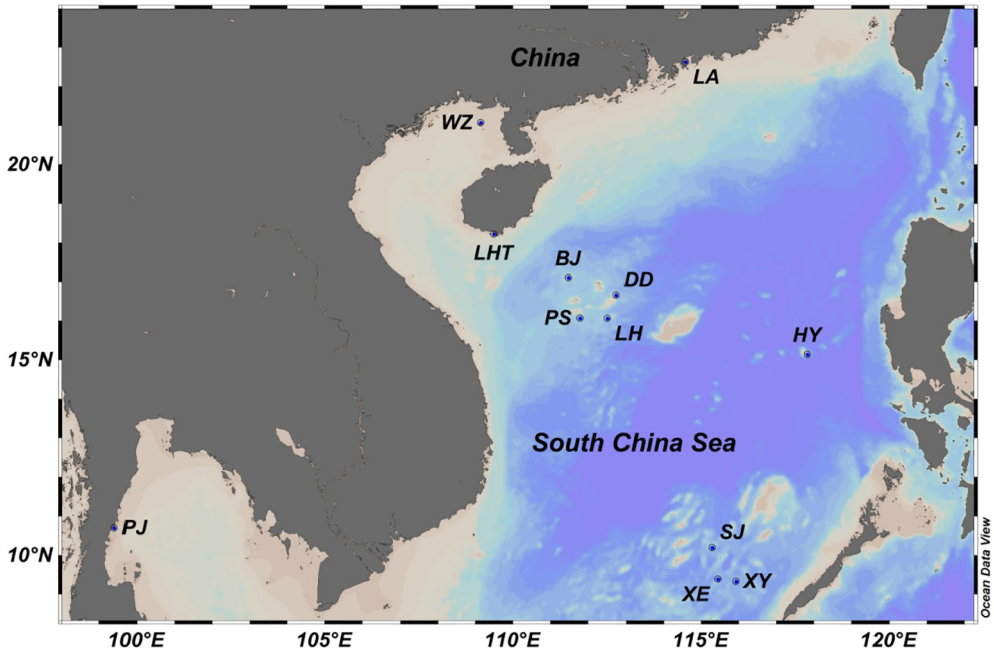

Fig. 1. Station map of 12 locations of coral reefs (LA, WZ, LHT, PJ, BJ, PS, LH, DD, HY, SJ, XE, and XY) in the SCS.

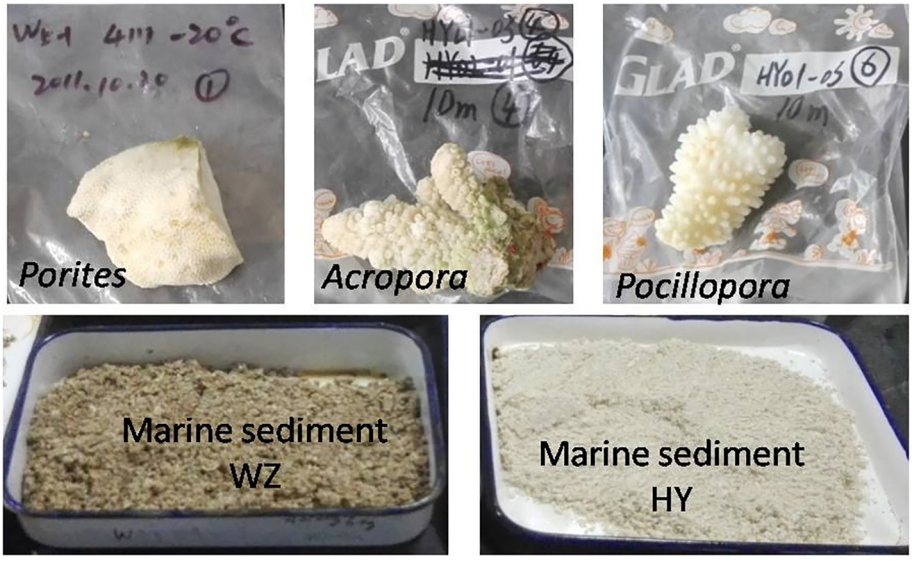

Fig. 2. Typical photo of marine sediments and coral skeletons in the SCS.

coral skeletons (length of 2–4 cm) collected from 12 coral reefs of the Lingao (LA), Weizhou Island (WZ), Luhuitou (LHT), Beijiao (BJ), Panshi (PS), Dongdao (DD), Langhua (LH), Huangyan Island (HY), Xinyi (XY), Xianer (XE), Sanjiao (SJ), and Puji (PJ) in the SCS. These stations were classified as the fringing reefs (LA, WZ, LHT, and PJ) in the coastal ocean and the atoll reefs (BJ, HY, XY, XE, PS, DD, LH, and SJ) in the open ocean. Two samples of marine sediments and a sample of living coral skeleton (*Porites*) were collected in the WZ during October 2015. Three samples of living coral skeleton (*Porites*, *Pocillopora*, and *Acropora*) and a sample of marine sediment were measured in the HY during May 2015. A sample of living coral skeleton (*Porites*) and two samples of marine sediments were sampled in the SJ during May 2016. A sample of coral skeleton and marine sediment each was simultaneously collected in the LA, LHT, and XE during May 2016. Only marine sediments were obtained in the PS, DD, LH, XY, BJ, and PJ. The station map and typical photo of samples are presented in Figs. 1 and 2. All sediments and coral skeletons were collected by SCUBA diving into ocean interior rather than by traditional grab sampling on shipboard. The coral polyps were rinsed immediately with deionized water after going back to the laboratory onboard. The coral skeletons and marine sediments were stored in a refrigerator (4 °C) before further analysis in a land-based laboratory.

Sediments and coral skeletons were dried in an oven at 60 °C. Shells and other exotic materials in marine sediments were eliminated. Coral skeletons were carefully chosen without evident bored and contaminated areas. Sediments and coral skeletons were pulverized into fine powder and sieved using an 80–100 mesh sieve. This pretreatment was consistent with those mentioned in other studies on marine sediments (Al-Qaradawi et al., 2015; Lin et al., 2018a; Lin et al., 2018b; Liu and Lin, 2018; Wang et al., 2015). These powders (100 g) were transferred into a cylindrical container and were sealed tightly to prevent the escape of radon for a period of over 30 days before the measurement of γ-spectrometry. The secular equilibrium of radium and its progenies was achieved and validated using standard materials before the

calculation of the activities of ^{226}Ra and ^{228}Ra through their progenies.

All the samples were measured by broad-energy high purity germanium (HPGe) γ-spectrometry (Canberra BE6530) with a relative efficiency of 63.4% and using Genie 2000 software. The detector is surrounded in sequence by 9.5 mm stainless iron, 150 mm lead, 1 mm tin, and 1.6 mm highly purified copper to significantly depress the background. The energy resolution (FWHM) is 1.58 keV at the photopeak of 1332 keV and is much better than energy resolution (~50 keV) of NaI γ-spectrometry in other studies (Ravisankar et al., 2015; Valan et al., 2016). The relative efficiency is derived from the standard river sediment (GBW08304a) and validated with the Irish Sea sediment (IAEA-385) with an identical size as that used in our samples. These standard sediments were produced by International Atomic Energy Agency (IAEA) and National Institute of Metrology of China. The detailed information about the above standard sediments could be referenced to other studies (Pham et al., 2008; Zhou et al., 2015).

Because of the particulate reactivity of ^{234}Th in the marine environment to constrain migration of ^{234}Th relative to its parent radionuclide ^{238}U (Lin et al., 2016b), the secular equilibrium between ^{238}U and ^{234}Th is generally observed in marine sediments. Additionally, the elapsed time between sampling date and measuring date was generally > 2 months in our study, thereby facilitating the secular equilibrium between ^{234}Th and ^{238}U in the samples at the measuring date. The γ-ray of 92.6 keV emitted from ^{234}Th is influenced by the γ-ray of 93.4 keV derived from ^{228}Ac. Therefore, the activity of ^{238}U was quantified by the photopeak of ^{234}Th (63.3 keV). The activity of ^{238}U was calculated using the γ-ray of ^{226}Ra and its progenies with the prerequirement of the secular equilibrium between ^{226}Ra and ^{238}U in other studies (LaBrecque et al., 2010; Valan et al., 2016). However, the disequilibrium of ^{226}Ra/^{238}U in marine sediments was also widely reported, especially for marine sediment in coral reefs (Liu and Lin, 2018). Therefore, we obtained the ^{238}U activity and its associated uncertainty based on the γ-ray of 63.3 keV rather than ^{226}Ra and its progenies according to Eqs. (1) and (2).

$$A^0_{238U} = \frac{(n_T - n_0)}{\varepsilon m} e^{\lambda_{238U}(t_1 - t_0)} \quad (1)$$

$$\delta A^0_{238U} = A^0_{238U} \times \sqrt{\frac{(n_T + n_0)}{T(n_T - n_0)^2}} \quad (2)$$

where, $A_{238U}{}^0$ and $\delta A_{238U}{}^0$ are the ^{238}U activity and uncertainty at the sampling date, respectively, and n_T and n_0 are the counting rates of the sample and background, respectively. The relative efficiency ε is derived from the standard river sediment and validated with that of the Irish Sea sediment (IAEA-385). t_1, t_0, and T are defined as the detection date, sampling date, and instrumental measurement time of the sample, respectively. The decay constant of ^{238}U refers to λ_{238U}. The uncertainty mainly originated from counting statistics and was represented as one standard deviation (1δ). The decay correction of ^{238}U from the measuring date to the sampling date could be neglected due to much long half-life of ^{238}U (4.47×10^9 a) relative to the elapsed time from the measuring date to the sampling date ($t_1 - t_0$). When the activity of ^{238}U was measured by γ-spectrometry, HPGe γ-spectrometry should be preferentially recommended rather than NaI γ-spectrometry because of the high background and low-energy resolution of NaI γ-spectrometry at the photopeak of 63.3 keV.

The activity of ^{226}Ra and uncertainty at the measuring date were calculated by the γ-rays of their progenies at the photopeaks of 351.9 keV (^{214}Pb/^{226}Ra) and 609.3 keV (^{214}Bi/^{226}Ra) based on the secular equilibrium of radium and its progenies according to Eqs. (3) and (4). However, the disequilibrium of ^{238}U-^{230}Th-^{226}Ra in carbonate sediments from coral reefs was reported in the previous studies (Lin et al., 2018b; Liu and Lin, 2018; Sam et al., 1998). We corrected the ^{226}Ra activity from the measuring date to sampling date according to Eqs. (5) and (6). The half-lives of ^{226}Ra (1.6×10^3 a) and ^{230}Th (7.7×10^4 a) were significantly longer than the elapsed time from the measuring date to sampling date (~1 a in this study). The decay and ingrowth correction was negligible in the ^{238}U-^{230}Th-^{226}Ra decay series in this study. Therefore, the ^{226}Ra activity and its uncertainty at the sampling date were approximately equal to those at the measuring date.

$$A_{226Ra} = \frac{(n_T - n_0)}{\varepsilon m} \quad (3)$$

$$\delta A_{226Ra} = A_{226Ra} \times \sqrt{\frac{(n_T + n_0)}{T(n_T - n_0)^2}} \quad (4)$$

$$A^0_{226Ra} = A_{226Ra} \times e^{\lambda_{226Ra}(t_1 - t_0)} - A^0_{238U} \times [e^{\lambda_{226Ra}(t_1 - t_0)} - e^{(\lambda_{226Ra} - \lambda_{230Th})(t_1 - t_0)}] \quad (5)$$

$$\delta A^0_{226Ra} = \sqrt{(\delta A_{226Ra})^2 \times e^{2\lambda_{226Ra}(t_1 - t_0)} + (\delta A^0_{238U})^2} \times [e^{\lambda_{226Ra}(t_1 - t_0)} - e^{(\lambda_{226Ra} - \lambda_{230Th})(t_1 - t_0)}]^2 \quad (6)$$

where, A_{226Ra} and δA_{226Ra} are the ^{226}Ra activity and its uncertainty on the measurement date, respectively. Other parameters are similar to the parameters given in Eqs. (1) and (2).

The activity of ^{228}Ra was obtained by the γ-ray (911.1 keV) of its daughter radionuclide (^{228}Ac) due to the short half-life of ^{228}Ac (6.13 h) and rapid equilibrium between ^{228}Ra and ^{228}Ac. The excess of ^{228}Th relative to ^{228}Ra in marine sediments has been reported in a previous study (Koide et al., 1973). We also found that the disequilibrium between ^{228}Th and ^{228}Ra was widely observed in coral reefs (our unpublished data). Therefore, the γ-rays of ^{228}Th and its progenies (238.6 keV, 583.2 keV, and 2614.5 keV) were not used to calculate the ^{228}Ra activity in this study. The ^{228}Ra activity and uncertainty were calculated by the γ-ray of 911.1 keV according to Eqs. (7) and (8).

$$A^0_{228Ra} = \frac{(n_T - n_0)}{\varepsilon m} e^{\lambda_{228Ra}(t_1 - t_0)} \quad (7)$$

$$\delta A^0_{228Ra} = A^0_{228Ra} \times \sqrt{\frac{(n_T + n_0)}{T(n_T - n_0)^2}} \quad (8)$$

where, $A_{228Ra}{}^0$ and $\delta A_{228Ra}{}^0$ refer to the ^{228}Ra activity and uncertainty at the sampling date. Other parameters were also similar to the parameters given in Eqs. (1) and (2).

The activity of ^{40}K and its associated uncertainty were directly calculated by its γ-ray of 1460.8 keV according to Eqs. (9) and (10). The half-life of ^{40}K (1.28×10^9 a) was also significantly longer than the elapsed time from the measuring date to the sampling date ($t_1 - t_0$). Therefore, the decay correction can also be neglected for the measurement of ^{40}K.

$$A^0_{40K} = \frac{(n_T - n_0)}{\varepsilon m} e^{\lambda_{40K}(t_1 - t_0)} \quad (9)$$

$$\delta A^0_{40K} = A^0_{40K} \times \sqrt{\frac{(n_T + n_0)}{T(n_T - n_0)^2}} \quad (10)$$

The minimum detection activity (MDA) was calculated using Eq. (11).

$$MDA = \frac{4.65}{\varepsilon m} \times \sqrt{\frac{n_0}{T}} \quad (11)$$

The definition of each parameter is consistent with that given in Eqs. (1) and (2). Under conditions of 100 g sediment and a measurement time of 2 days, the MDA of ^{228}Ra though Canberra BE6530 was ~1.0 Bq/kg.

For analytical quality control, the standard sediment of IAEA-385 was analyzed using the relative efficiency derived from the standard river sediment (GBW08304a). The obtained value was consistent with the reference value of IAEA-385 corrected to April 18, 2017 (Table 1). The instrumental background and detection efficiency were periodically measured to guarantee the data quality. We also participated in and passed the proficiency test for radionuclides (^{210}Pb, ^{238}U, ^{226}Ra,

Table 1
Comparison of the obtained value using the standard sediment of GBW08304a and the reference value in IAEA-385. Uncertainty of activity was reported by one standard deviation with the confidence level of 68% (unit: Bq/kg).

Radionuclides	Photopeak (keV)	Obtained value based on GBW08304a		Reference value of IAEA-385 (corrected to 4/18, 2017)
		Raw value	Mean value	
^{238}U	63.3	30.8 ± 2.7	30.8 ± 2.7	29.0 ± 0.5
^{226}Ra	295.1	19.2 ± 0.9	20.6 ± 1.4	21.9 ± 0.2
	352.0	20.4 ± 0.7		
	609.3	22.1 ± 1.2		
^{137}Cs	661.7	20.1 ± 0.5	20.1 ± 0.5	20.2 ± 0.2

^{228}Ra, ^{228}Th, ^{40}K, and ^{137}Cs) in marine sediments organized by the National Marine Environmental Monitoring Center of China in October 2017.

We measured radioactivity simultaneously in surface marine sediments and living coral skeletons collected from the fringing reefs (LA, WZ, LHT, and PJ) and atoll reefs (BJ, PS, DD, LH, HY, XY, XE, and SJ) in the SCS (Table 2). Overall, the average radioactivity in marine sediments and coral skeletons was in the order of ^{238}U (27.7 Bq/kg) > ^{40}K (9.28 Bq/kg) > ^{228}Ra (3.00 Bq/kg) > ^{226}Ra (2.80 Bq/kg) and ^{238}U (31.7 Bq/kg) > ^{40}K (13.9 Bq/kg) > ^{228}Ra (8.89 Bq/kg) > ^{226}Ra (3.06 Bq/kg), respectively. By contrast, the order of ^{40}K (400 Bq/kg) > ^{238}U (35 Bq/kg) = ^{226}Ra (35 Bq/kg) > ^{228}Ra (30 Bq/kg) is generally observed in the global soil and sediment (Lin et al., 2016b; UNSCEAR, 2000).

The activity of ^{238}U in coral skeletons and marine sediments (22 Bq/kg–43 Bq/kg) based on HPGe γ-spectrometry in this study was consistent with the ^{238}U activity (25 Bq/kg–43 Bq/kg) measured by thermal ionization mass spectrometry (TIMS) and multi-collector inductively coupled plasma mass spectrometry (MC-ICPMS) in the SCS (L. Wang et al., 2017; Yu et al., 2010). Additionally, no significant difference in ^{238}U activity between marine sediments (27.7 ± 5.0 Bq/kg) and coral skeletons (31.7 ± 7.3 Bq/kg) was observed in coral reef systems.

In the present study, the activity of ^{40}K ranged from 2 Bq/kg to 27 Bq/kg in marine sediments and coral skeletons, excluding high ^{40}K activity in marine sediments (154 Bq/kg) at the station LA located in the fringing reef. The significantly high ^{40}K activity at coastal station LA may be attributed to the proximity to the mainland of Southern China and the contribution of other terrigenous minerals such as K-feldspar ($KAlSi_3O_8$) and mica ($KAlSi_4O_{10}$) weathering from granite characterized by high radioactivity (Patiris et al., 2016; Xia et al., 2013). The terrigenous minerals of K-feldspar and illite were directly observed by X-ray diffraction analysis and contributed to 45.9% of mass in the sinking particle in the fringing reef (Zhao et al., 2013).

The concentration of K was measured to be 0.1–0.4 g/kg (equivalent to 3–12 Bq/kg of ^{40}K) by inductively coupled plasma-optical emission spectrometry (ICP-OES) in the SCS (Xu et al., 2011). The activity of ^{40}K in coral-based soil was also reported to be 10.7 ± 0.5 Bq/kg (200 samples) on the Marshall Islands (Simon et al., 2002). Results of both of the above-mentioned studies were similar to our results of ^{40}K in marine sediments (9.28 Bq/kg excluding the station LA). The cold-water coral skeleton had the ^{40}K activity of 0.13–1.4 Bq/kg (Sabatier et al., 2012), which was lower than ^{40}K activity (13.9 Bq/kg) in hermatypic coral skeleton living in shallow water (Table 2). The elevated ^{40}K activity in hermatypic coral skeleton relative to cold-water coral skeleton may be attributed to the distinct coral genera with different mineral components and concentration factor (CF) to take up ^{40}K from seawater. Overall, the ^{40}K activity in the coral skeleton (13.9 ± 6.7 Bq/kg) was also similar to that in the marine sediment (9.28 ± 5.40 Bq/kg).

The concentration of ^{226}Ra is generally ~10^{-8} ppm (equivalent to 0.37 Bq/kg) relative to 2 ppm–4 ppm of ^{238}U (equivalent to 25 Bq/kg-50 Bq/kg) in coral skeletons. Radium isotope is generally measured using radiometric instruments (e.g. HPGe γ-spectrometry) rather than mass spectrometry. As the concentration of radium isotope is generally lower than the limit of detection for mass spectrometry because of the short half-life of radium relative to that of uranium (Hsieh and Henderson, 2011), the data of ^{226}Ra and ^{228}Ra are very limited relative to ^{238}U in hermatypic coral skeletons. In the present study, the average activities of ^{226}Ra and ^{228}Ra were 3.06 Bq/kg and 8.89 Bq/kg in coral

Table 2
Radioactivity in marine sediments and coral skeletons. Uncertainty of activity was reported by one standard deviation with the confidence level of 68% (unit: Bq/kg).

Station	Matrixes		^{238}U	^{40}K	^{226}Ra	^{228}Ra
SJ	Marine sediment	SJ01	23.6 ± 1.7	10.8 ± 0.5	2.31 ± 0.22	1.67 ± 0.58
		SJ03	24.1 ± 1.7	8.72 ± 0.42	2.08 ± 0.22	1.62 ± 0.63
		SJ05	25.0 ± 2.5	7.93 ± 0.44	1.95 ± 0.33	1.65 ± 0.61
		Mean	24.2 ± 0.7	9.16 ± 1.49	2.11 ± 0.18	1.65 ± 0.03
	Coral skeleton	*Porites*	25.3 ± 1.8	6.74 ± 0.35	2.07 ± 0.17	8.20 ± 0.76
HY	Marine sediment		38.2 ± 4.8	2.15 ± 0.71	1.66 ± 0.15	< 1.00[a]
	Coral skeleton	*Porites*	31.4 ± 4.0	12.2 ± 1.5	2.51 ± 0.34	4.68 ± 0.68
		Pocillopora	38.8 ± 4.8	14.5 ± 1.4	1.82 ± 0.23	2.87 ± 0.45
		Acropora	36.9 ± 4.6	18.1 ± 1.9	2.01 ± 0.29	2.67 ± 0.49
		Mean	35.7 ± 3.8	15.0 ± 3.0	2.11 ± 0.36	3.41 ± 1.11
WZ	Marine sediment	W2-2	36.2 ± 4.7	11.9 ± 1.3	2.38 ± 0.34	3.11 ± 0.54
		W5-1	33.3 ± 4.1	12.8 ± 1.1	2.96 ± 0.32	3.87 ± 0.49
		Mean	34.8 ± 2.1	12.3 ± 0.7	2.67 ± 0.41	3.49 ± 0.54
	Coral skeleton	*Porites*	42.5 ± 5.3	15.2 ± 1.5	3.25 ± 0.42	27.3 ± 3.0
XE	Marine sediment	XE-01	23.6 ± 1.7	10.8 ± 0.5	2.31 ± 0.22	1.66 ± 0.58
	Coral skeleton	*Porites*	23.4 ± 1.7	8.04 ± 0.39	3.68 ± 0.22	8.84 ± 0.81
LHT	Marine sediment	LHT-D1	32.2 ± 4.1	23.1 ± 2.1	3.02 ± 0.40	4.42 ± 0.67
	Coral skeleton	*Porites*	23.7 ± 2.3	27.5 ± 1.14	6.46 ± 0.36	8.17 ± 1.15
LA	Marine sediment	LA-2	26.3 ± 3.2	154 ± 10	9.39 ± 0.89	14.4 ± 1.6
	Coral skeleton	*Acropora*	32.0 ± 4.0	7.62 ± 1.18	2.34 ± 0.36	7.83 ± 1.13
XY	Marine sediment	XY-01	25.9 ± 2.0	2.54 ± 0.16	1.64 ± 0.22	1.17 ± 0.55
BJ	Marine sediment	BJ01-03	22.1 ± 2.7	3.36 ± 0.54	1.47 ± 0.19	0.63 ± 0.12
PS	Marine sediment	PS1-6	26.9 ± 1.5	12.5 ± 0.5	1.06 ± 0.07	1.75 ± 0.16
DD	Marine sediment	DD2-5	23.0 ± 2.0	8.09 ± 0.48	2.27 ± 0.18	1.37 ± 0.74
LH	Marine sediment	LH2-5	25.9 ± 2.7	10.3 ± 0.7	2.47 ± 0.24	1.66 ± 0.18
PJ	Marine sediment	T1	29.3 ± 2.6	4.93 ± 0.37	4.99 ± 0.44	5.52 ± 0.97

[a] " < " indicates that the activity is lower than that of MDA according to Eq. (11).

skeletons and 2.80 Bq/kg and 3.00 Bq/kg in marine sediments.

It was reported that the ^{226}Ra and ^{228}Ra activities were 0.7 Bq/kg–4.8 Bq/kg and 0.3 Bq/kg–3 Bq/kg in *Solenastrea* coral skeleton from the Atlantic Ocean, respectively (Moore and Krishnaswami, 1972). Our results of ^{226}Ra and ^{228}Ra were 1.82 Bq/kg–6.46 Bq/kg and 2.67 Bq/kg–27.3 Bq/kg in the SCS, respectively, which were higher than the results in the Atlantic Ocean (Moore and Krishnaswami, 1972). The activity of radium isotope greatly depends on its terrestrial sources from river, submarine groundwater discharge, and sediment (Moore, 2010). The marginal sea of the SCS is surrounded by the Asian continent and islands in Southeastern Asia and is highly influenced by the terrestrial inputs relative to the Atlantic Ocean, probably resulting in higher activity of radium isotope in coral skeletons collected from the SCS. It was worth noting that the activity of ^{228}Ra in the coral skeleton (27.3 Bq/kg) was significantly high in the WZ in the coastal ocean when compared with that of other coral skeletons (2.67 Bq/kg–8.84 Bq/kg) in the open ocean. The activity of ^{228}Ra greatly depends on terrestrial sources and is more variable than that of ^{226}Ra in the global ocean (Cho and Kim, 2016). The ^{228}Ra activity was also observed to be higher in the coastal seawater (30 Bq/m^3) than in the open ocean (2 Bq/m^3–3 Bq/m^3) in the SCS (Nozaki and Yamamoto, 2001; Wang and Du, 2016). This high ^{228}Ra activity in the coral skeleton (WZ) may be attributed to the uptake of high ^{228}Ra activity from the surrounding coastal seawater into the coral skeleton.

The average ^{226}Ra activity in the coral skeleton (3.06 ± 1.50 Bq/kg) was consistent with that in the marine sediment (2.80 ± 2.04 Bq/kg). By contrast, the average ^{228}Ra activity in the coral skeleton (8.89 ± 7.85 Bq/kg) was higher than that in the marine sediment (3.00 ± 3.46 Bq/kg). The contrasting patterns of ^{226}Ra and ^{228}Ra activities were determined by the physical half-life (1600 a for ^{226}Ra and 5.75 a for ^{228}Ra). The living coral skeleton was freshly accreted by coral polyps. The radium isotopes (^{228}Ra and ^{226}Ra) in seawater were simultaneously incorporated into the coral skeleton along with Ca and Sr in the same group of alkaline earth elements. Marine sediment in the coral reef region was mainly fragmented and weathered from the coral skeleton, especially for the atoll reefs in the center of the SCS. The elapsed time occurs during the transformation of coral skeleton into carbonate sediment in coral reefs. The half-life of ^{226}Ra (1600 a) was much longer than the elapsed time, which resulted in no difference of ^{226}Ra activity in marine sediments and coral skeletons during the formation of marine sediment from coral skeleton in the atoll reefs. Furthermore, similar activity in marine sediment and coral skeleton was also observed for other long half-life radionuclides of ^{238}U (4.47×10^9 a) and ^{40}K (1.28×10^9 a) in this study. However, the ^{228}Ra activity will decay away if the elapsed time is longer than the half-life of ^{228}Ra (5.75 a), thereby resulting in low ^{228}Ra activity in marine sediments relative to high ^{228}Ra activity in living coral skeletons.

Marine sediment, which is mainly originated from reef-building coral skeleton in coral islands, can be transferred to beach and plays a critical role in beach nourishment to adapt to the sea-level rising (SLR). However, the elapsed time scale of the formation of marine sediment from coral skeleton is poorly investigated and constraint in coral reef systems. In the present study, the high ^{228}Ra activity in coral skeleton relative to surface marine sediment may be used to constrain this elapsed time according to Eq. (12). Deviation of the elapsed time may be introduced due to other contributions of ^{228}Ra in marine sediment from the terrestrial minerals with high ^{228}Ra activity. We mainly focused on marine sediment in atoll reefs (SJ, HY, and XE) far from the continents in this study to eliminate the influence of terrigenous materials. The preliminary results of the elapsed time were 13.3 a, 15.9 a, and 13.9 a in the atoll reefs of SJ, HY, and XE, respectively, with very limited terrestrial inputs.

$$t = \frac{1}{\lambda_{228Ra}} \ln \frac{A^{228Ra}_{Coral}}{A^{228Ra}_{Sediment}} \quad (12)$$

Considering the sedimentation rate in the marine sediment (~0.1 cm/a) derived from the ^{14}C dating method in coral reefs located in the SCS (Yu et al., 2009), the age of the surface marine sediment (within 2 cm from the top) was at the time scale of 0–20 a. The elapsed time of surface sediments based on ^{228}Ra was in the range of the age based on the ^{14}C dating method in the surface marine sediment. Although the preliminary results of the elapsed time based on ^{228}Ra may provide a clue to constrain the time scale of the formation of marine sediment, much work is needed to narrow down uncertainty of the elapsed time.

The activity ratio of ^{226}Ra to ^{238}U in marine sediment was used to identify the source of materials (Huang et al., 2013; Lin et al., 2018b; J. Wang et al., 2017). The variation of the activity ratio of ^{226}Ra to ^{238}U depends on the local geology and geochemical settings of the area (Liu and Lin, 2018). In the present study, we found abnormally low ^{226}Ra/^{238}U activity ratio in the marine sediment in coral reefs. The atoll reefs had the ^{226}Ra/^{238}U activity ratio ranging from 0.04 to 0.10 with the mean ratio of 0.08. The ^{226}Ra/^{238}U activity ratio ranged from 0.07 to 0.36 with the average value of 0.16 in the fringing reefs. Overall, the ^{226}Ra/^{238}U activity ratio in coral reefs was significantly lower than ^{226}Ra/^{238}U activity ratio in the mangroves and seagrass obtained in our previous study (Liu and Lin, 2018).

Most of the ^{226}Ra/^{238}U activity ratios were lower than 0.10 in coral reefs excluding the fringing reefs (0.36 at the station LA), which is significantly influenced by the terrigenous minerals. It was noted that a high ^{40}K activity (154 Bq/kg) was also coincided with a high ^{226}Ra/^{238}U ratio (0.36) at the station LA. The activity ratio of ^{226}Ra to ^{238}U ranged from 0.5 to 1.0 in other marine sediments collected from Laizhou Bay (Wang et al., 2015), Yangtze Estuary (J. Wang et al., 2017), Daya Bay (Zhou et al., 2015), Hong Kong (Yu et al., 1994), and Guanghai Bay (Zhao et al., 2015) along the coastline of China. The activity ratio of ^{226}Ra to ^{238}U in soil and sand was also reported to be higher than 1.0 from Malaysia (1.76–2.33) (Almayahi et al., 2012). The relationship between ^{226}Ra and ^{238}U from different sea areas is presented in Fig. 3.

The ^{226}Ra/^{238}U activity ratio in marine sediment (0.5–1.0) outside coral reefs is generally attributed to the ingrowth process of the ^{238}U-^{230}Th-^{226}Ra decay chain in terrigenous minerals with an “old” age to reach equilibrium/quasi-equilibrium in ^{238}U-series after its transformation and transferring from the Earth's Interior (Fig. 4). However, the unique feature of abnormally low ^{226}Ra/^{238}U ratio ($k < 0.1$) in coral reefs is attributed to the biological process of active uptake of ^{226}Ra and ^{238}U from seawater by coral polyps rather than the physical process of the ^{238}U-^{230}Th-^{226}Ra decay chain.

Considering the sedimentation rate (~0.1 cm/a) in the marine sediment of coral reefs in the SCS (Yu et al., 2009), the depth of the marine sediment (0 cm–2 cm) corresponds to the time scale of 0–20 a for the age of the marine sediment. The radionuclide of ^{230}Th has a low activity in seawater and is also greatly rejected in living coral skeleton (Cobb et al., 2003), thereby resulting in a low ^{230}Th activity ($< 10^{-3}$ Bq/kg) in living coral skeleton and marine sediment mainly originating from the coral skeleton. If the ^{238}U activity (50 Bq/kg) and elapsed time (10 a) are assumed, the activity of ^{226}Ra ingrowth from the ^{238}U-^{230}Th-^{226}Ra decay chain will be $\sim 9.7 \times 10^{-6}$ Bq/kg according to Eq. (13). The ^{226}Ra/^{238}U ratio should be $\sim 10^{-7}$ in marine sediment based on the above assumption of ^{238}U (50 Bq/kg) and ^{226}Ra ($\sim 9.7 \times 10^{-6}$ Bq/kg). Both the ^{226}Ra activity (9.7×10^{-6} Bq/kg) and ^{226}Ra/^{238}U activity ratio (10^{-7}) are significantly lower than ^{226}Ra activity (1 Bq/kg–4 Bq/kg) and ^{226}Ra/^{238}U ratio (0.04–0.10) obtained in this study. Therefore, the ^{226}Ra and ^{226}Ra/^{238}U ratio cannot be explained by the physical process of the ^{238}U-^{230}Th-^{226}Ra decay chain.

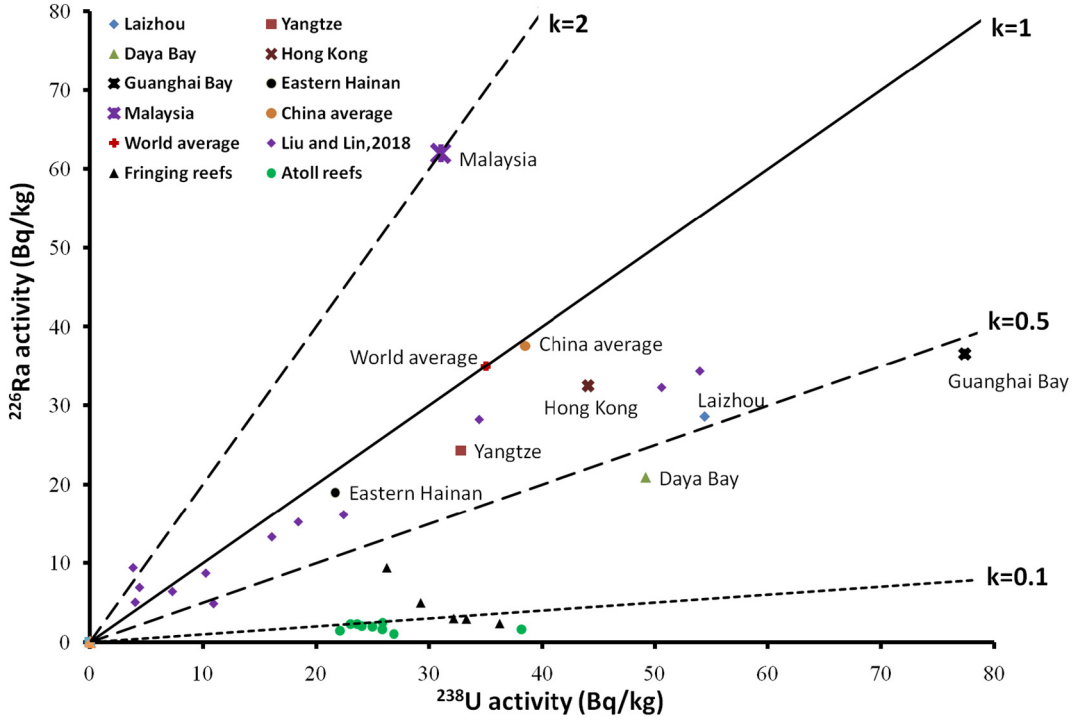

Fig. 3. Relationship between ^{226}Ra and ^{238}U in marine sediment. k means the activity ratio of ^{226}Ra to ^{238}U. The activity ratio of ^{226}Ra/^{228}Ra was < 0.1 in most regions of coral reefs and was lower than our previous results in Liu and Lin (2018) and other sea areas, the references of which are cited in the text.

$$A_{226Ra} = \frac{\lambda_{226Ra}\lambda_{230Th}A_{238U}e^{-\lambda_{238U}\times t}}{(\lambda_{230Th}-\lambda_{238U})(\lambda_{226Ra}-\lambda_{238U})} + \frac{\lambda_{226Ra}\lambda_{230Th}A_{238U}e^{-\lambda_{230Th}\times t}}{(\lambda_{238U}-\lambda_{230Th})(\lambda_{226Ra}-\lambda_{230Th})} + \frac{\lambda_{226Ra}\lambda_{230Th}A_{238U}e^{-\lambda_{226Ra}\times t}}{(\lambda_{230Th}-\lambda_{226Ra})(\lambda_{238U}-\lambda_{226Ra})} \quad (13)$$

The ^{226}Ra and ^{238}U activities of seawater are approximately 1 Bq/m^3–3 Bq/m^3 and 40 Bq/m^3 in the SCS (W.H. Lin et al., 2015). The concentration factor (CF) of ^{226}Ra and ^{238}U is ~1000 L/kg for reef-building corals (Baskaran, 2012; Saha et al., 2016). The ^{226}Ra and ^{238}U activities of coral skeleton are approximately 1 Bq/kg–3 Bq/kg and 40 Bq/kg, respectively, according to Eqs. (14) and (15), which are consistent with our results (Table 2). The ^{226}Ra/^{238}U ratio is calculated to be 0.03–0.08, which is also similar to our field measurements (0.04–0.10). Consequently, the biological process of active uptake of ^{226}Ra and ^{238}U from seawater by coral polyp contributed to the ^{226}Ra activity and ^{226}Ra/^{238}U ratio in coral skeleton and marine sediment in coral reefs.

$$^{226}Ra|_{coral\ skeleton} = {}^{226}Ra|_{seawater} \times CF_{226Ra} \quad (14)$$

$$^{238}U|_{coral\ skeleton} = {}^{238}U|_{seawater} \times CF_{238U} \quad (15)$$

Overall, coral reefs have a specific endmember with regard to the activity ratio of ^{226}Ra to ^{238}U (< 0.1), which may be used to investigate the contributions of biogenic carbonate sediments and terrigenous sediment with the distinct ^{226}Ra/^{238}U activity ratios in the fringing reefs. The ^{226}Ra/^{238}U activity ratio may be a valuable proxy for tracking the terrigenous particle carried by rivers, which had been indicated to threaten the health of the coral reef ecosystem (McCulloch et al., 2003).

Several exposure pathways of radionuclides, including seafood consumption, house construction with the reef rock, and SCUBA diving, occur and result in ionizing radiation exposure to humans. The dominant component of ionizing radiation generally originates from naturally occurring radionuclides rather than artificial radionuclides (UNSCEAR, 2000). As there was no record of nuclear weapons testing and nuclear accident in the SCS, the amount of artificial radionuclides

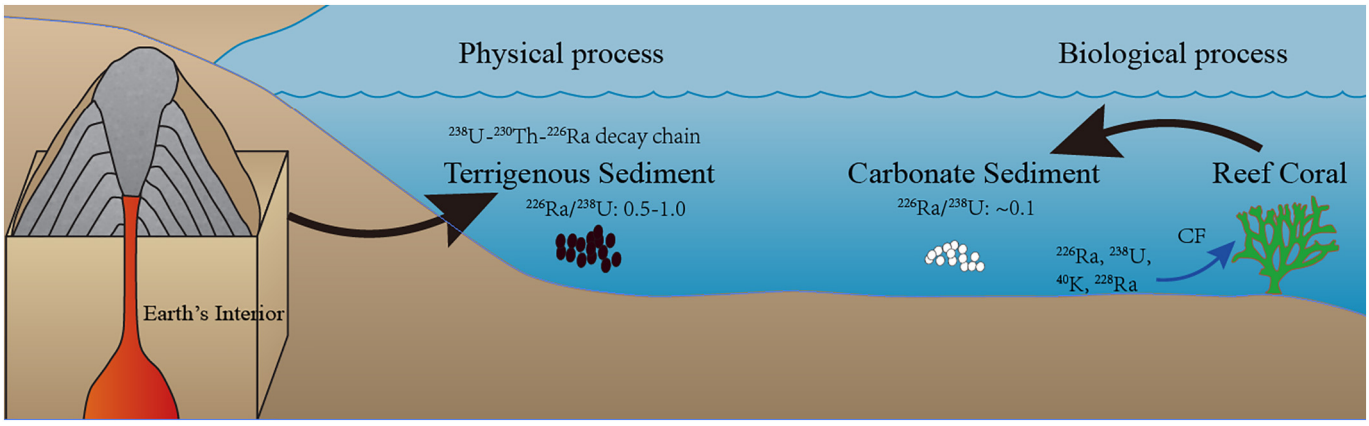

Fig. 4. Contrasting patterns of ^{226}Ra/^{238}U activity ratio in marine sediments from coral reefs and other marine environments outside coral reefs.

Table 3
Radiological hazards assessment in coral reefs.

Station	Matrixes	^{226}Ra (Bq/kg)	^{228}Ra (Bq/kg)	^{40}K (Bq/kg)	Ra_{eq} (Bq/kg)	H_{ex}	H_{in}	$I_{\gamma r}$	D_R (nGy/h)	AEDE (mSv/y)
SJ	Marine sediment	2.11 ± 0.18	1.65 ± 0.03	9.16 ± 1.49	5.17	0.01	0.02	0.04	2.36	2.89×10^{-3}
	Coral skeleton	2.07 ± 0.17	8.20 ± 0.76	6.74 ± 0.35	14.3	0.04	0.04	0.10	6.19	7.59×10^{-3}
HY	Marine sediment	1.66 ± 0.15	0.50[a]	2.15 ± 0.71	2.54	0.01	0.01	0.02	1.16	1.42×10^{-3}
	Coral skeleton	2.11 ± 0.36	3.41 ± 1.11	15.0 ± 3.0	8.14	0.02	0.03	0.06	3.66	4.49×10^{-3}
WZ	Marine sediment	2.67 ± 0.41	3.49 ± 0.54	12.3 ± 0.7	8.61	0.02	0.03	0.06	3.86	4.73×10^{-3}
	Coral skeleton	3.25 ± 0.42	27.3 ± 3.0	15.2 ± 1.5	43.4	0.12	0.13	0.30	18.6	2.28×10^{-2}
XE	Marine sediment	2.31 ± 0.22	1.66 ± 0.58	10.8 ± 0.5	5.52	0.01	0.02	0.04	2.53	3.10×10^{-3}
	Coral skeleton	3.68 ± 0.22	8.84 ± 0.81	8.04 ± 0.39	17.0	0.05	0.06	0.12	7.38	9.05×10^{-3}
LHT	Marine sediment	3.02 ± 0.40	4.42 ± 0.67	23.1 ± 2.1	11.1	0.03	0.04	0.08	5.03	6.17×10^{-3}
	Coral skeleton	6.46 ± 0.36	8.17 ± 1.15	27.5 ± 1.1	20.3	0.05	0.07	0.14	9.07	1.11×10^{-2}
LA	Marine sediment	9.39 ± 0.89	14.4 ± 1.6	154 ± 910	41.9	0.11	0.14	0.31	19.5	2.39×10^{-2}
	Coral skeleton	2.34 ± 0.36	7.83 ± 1.13	7.62 ± 1.18	14.1	0.04	0.04	0.10	6.13	7.52×10^{-3}
XY	Marine sediment	1.64 ± 0.22	1.17 ± 0.55	2.54 ± 0.16	3.51	0.01	0.01	0.02	1.57	1.93×10^{-3}
BJ	Marine sediment	1.47 ± 0.19	0.63 ± 0.12	3.36 ± 0.54	2.63	0.01	0.01	0.02	1.20	1.47×10^{-3}
PS	Marine sediment	1.06 ± 0.07	1.75 ± 0.16	12.5 ± 0.5	4.52	0.01	0.02	0.03	2.07	2.54×10^{-3}
DD	Marine sediment	2.27 ± 0.18	1.37 ± 0.74	8.09 ± 0.48	4.85	0.01	0.02	0.03	2.22	2.72×10^{-3}
LH	Marine sediment	2.47 ± 0.24	1.66 ± 0.18	10.3 ± 0.7	5.64	0.02	0.02	0.04	2.58	3.16×10^{-3}
PJ	Marine sediment	4.99 ± 0.44	5.52 ± 0.97	4.93 ± 0.37	13.3	0.04	0.05	0.09	5.84	7.17×10^{-3}
Recommended value (Ravisankar et al., 2015)					370	1	1	0.5	84	0.46

[a] Half of the MDA (1.00 Bq/kg) is used for radiological hazard assessment.

originating from global fallout was also very limited relative to that of naturally occurring radionuclides in the SCS. The activities of most concerning artificial radionuclides of ^{137}Cs (< 0.07 Bq/kg), ^{90}Sr (~1.0 Bq/kg), and $^{239+240}$Pu (10^{-2} Bq/kg) were lower than those of naturally occurring radionuclides of ^{238}U (22 Bq/kg-43 Bq/kg), ^{40}K (2 Bq/kg-27 Bq/kg), ^{228}Ra (2.67 Bq/kg-27.3 Bq/kg), and ^{226}Ra (1.82 Bq/kg-6.46 Bq/kg) in coral reefs (Lindahl et al., 2011; Xu et al., 2010). Therefore, radiological hazard assessment was conducted from the fringing reefs in the coastal ocean to atoll reefs in the open ocean based on the results of naturally occurring radionuclides. The radiological indices including radium equivalent activity (Ra_{eq}), external and internal hazard indices (H_{ex} and H_{in}), representative gamma level index ($I_{\gamma r}$), absorbed gamma dose rate (D_R), and annual effective dose equivalent (AEDE) were calculated according to Eqs. (16)–(21) and data are represented in Table 3 (Liu and Lin, 2018). Table 3 also shows recommended values of the radiological parameters for comparison. Note that no error was provided for these indices for environmental radiation assessment and management.

$$Ra_{eq}(Bq/kg) = A_{Ra} + 1.43A_{Th} + 0.077A_K \quad (16)$$

$$H_{ex} = \frac{A_{Ra}}{370} + \frac{A_{Th}}{259} + \frac{A_K}{4810} \quad (17)$$

$$H_{in} = \frac{A_{Ra}}{185} + \frac{A_{Th}}{259} + \frac{A_K}{4810} \quad (18)$$

$$I_{\gamma r} = \frac{A_{Ra}}{150} + \frac{A_{Th}}{100} + \frac{A_K}{1500} \quad (19)$$

$$D_R\,(nGy/h) = 0.462A_{Ra} + 0.604A_{Th} + 0.042A_K \quad (20)$$

$$AEDE(mSv/y) = D_R\,(nGy/h) \times 8760(h^{-1}) \times 0.7(Sv/Gy) \times 0.2 \times 10^{-6} \quad (21)$$

Consistent with other studies (Al-Qaradawi et al., 2015; Uddin and Behbehani, 2018; J. Wang et al., 2017), the activity of ^{232}Th could not be directly measured by HPGe γ-spectrometry and was conservatively substituted for by its daughter radionuclide ^{228}Ra activity during radiological hazard assessment. Note that the ^{232}Th activity in the coral skeleton (< 10^{-3} Bq/kg) is generally lower than ^{228}Ra activity (2.67 Bq/kg-27.3 Bq/kg Bq/kg) during the growth of reef-building coral (Cobb et al., 2003). Therefore, radiological hazard assessment will be conservatively overestimated due to the excess ^{228}Ra relative to ^{232}Th in the coral skeleton. Even so, all the values of radiological parameters were significantly lower than the recommended values in Table 3.

All the above radiological indices were calculated depending on the activities of the same naturally occurring radionuclides (^{226}Ra, ^{228}Ra, and ^{40}K), and we achieved consistent results for these indices. In the following discussion, we mainly focus on the typical parameter of Ra_{eq}. The value of Ra_{eq} was higher in coral skeletons than in marine sediments (Fig. 5). Similar activities of ^{226}Ra and ^{40}K were observed in coral skeletons and marine sediments in coral reefs. Therefore, a high value of Ra_{eq} in coral skeleton was mainly determined by high ^{228}Ra activity in coral skeletons relative to marine sediments.

The value of Ra_{eq} was higher in the fringing reefs than in the atoll reefs (Fig. 6). The average Ra_{eq} in marine sediments collected from the fringing reefs was 18.7 Bq/kg relative to 4.30 Bq/kg from the atoll reefs.

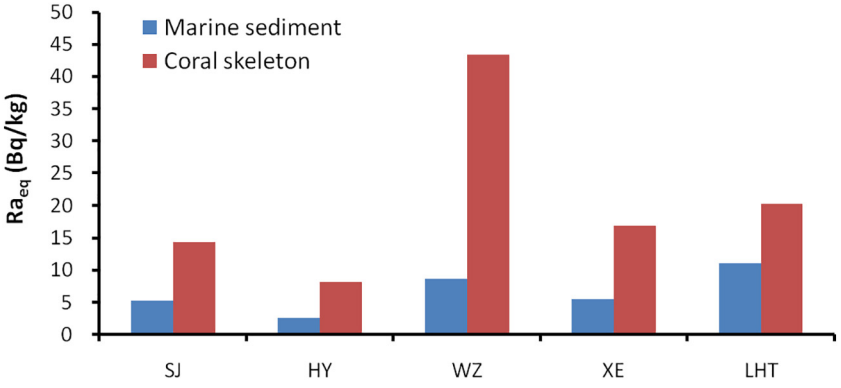

Fig. 5. Simultaneous results of Ra_{eq} in the coral skeleton and the marine sediment in coral reefs.

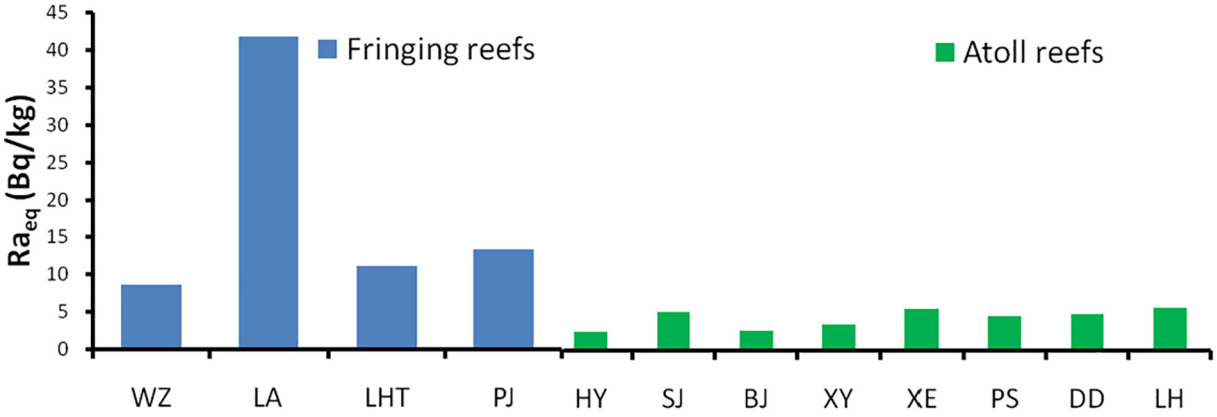

Fig. 6. Ra_{eq} in marine sediments from the fringing reefs (LA, WZ, LHT, and PJ) to the atoll reefs (HY, SJ, BJ, XY, XE, PS, DD, and LH).

The aforesaid high value in the fringing reefs may be attributed to its influence by the terrigenous minerals with high radioactivity relative to the atoll reefs in the center of the SCS. The high value of Ra_{eq} in the marine sediment (Fig. 6), which coincided with high ^{40}K (154 Bq/kg) and high $^{226}Ra/^{238}U$ activity ratio (0.36), was observed at the station LA and probably related to the terrestrial inputs. The external contributions of other terrigenous minerals would have also elevated radioactivity in the marine sediment located in the fringing reefs by human activity and river input, such as K-feldspar ($KAlSi_3O_8$), mica ($KAlSi_4O_{10}$), monazites [$(Ce_4LaTh)PO_4$], and zircons [$Zr(UTh)SiO_4$] weathering from granite characterized by high radioactivity (Patiris et al., 2016; Xia et al., 2013).

Radionuclides were reported in other marine sediments from Laizhou Bay (Wang et al., 2015), Yangtze Estuary (J. Wang et al., 2017), Daya Bay (Zhou et al., 2015), Hong Kong (Yu et al., 1994), and Guanghai Bay (Zhao et al., 2015) along the coastline of China. The integrated radioactivity was calculated using Eq. (16) and is presented in Fig. 7. The Ra_{eq} of the China's average and world's average was also calculated according to activities from other references and compared with that of marine sediments in coral reefs (UNSCEAR, 2000; Wang, 2002). The Ra_{eq} of marine sediment in coral reefs (2 Bq/kg–42 Bq/kg) was one order or two orders of magnitude lower than that in other sea areas, the world's average and China's average (109–164 Bq/kg). It was noted that the mean value of Ra_{eq} in the atoll reefs (4.30 Bq/kg) was < 5% of Ra_{eq} of the world's average (109 Bq/kg). Therefore, marine sediment in coral reefs has a unique low value of Ra_{eq}, which was attributed to biogenic carbonate sediment mainly originating from the fragment and weathering of coral skeleton relative to other marine sediments ultimately originating from the Earth's interior after a series of physical and geological processes. Note that the mechanism of low radioactivity in coral reefs is different from that of low concentration of other hazardous materials (antibiotics and perfluoroalkyl substances). For example, a low concentration of antibiotics and perfluoroalkyl substances in coral reefs was mainly attributed to limited human

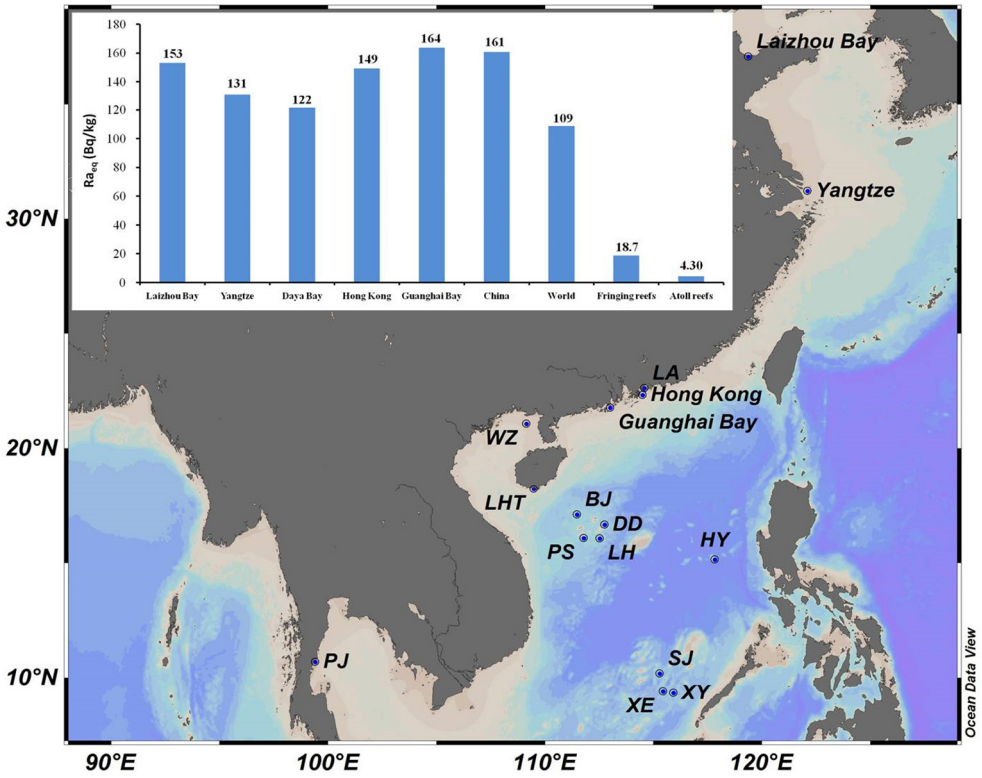

Fig. 7. Ra_{eq} of marine sediment in coral reefs (fringing reefs and atoll reefs) and other sea areas. The world's average and China's average were also calculated for comparing. The activities of naturally occurring radionuclides that were used to calculate Ra_{eq} were derived from other references that are cited in the text.

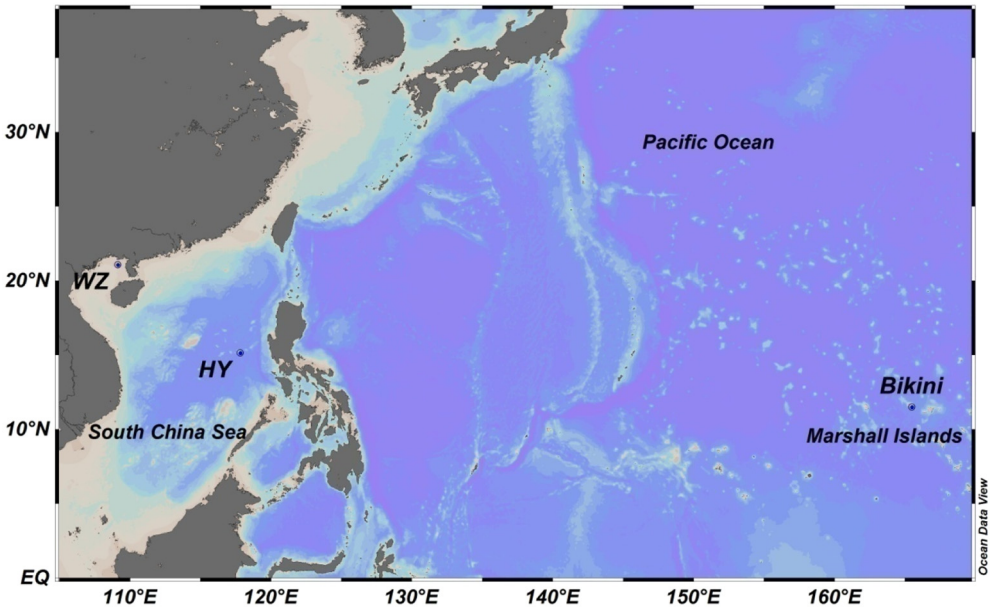

Fig. 8. Station map of Bikini Atolls and Huangyan Island (HY).

activity (Pan et al., 2018; Zhang et al., 2018).

Much work has been conducted on searching extremely high background radiation areas (HBRA) in the terrestrial habitats from the perspective of health physics (Shuaibu et al., 2017; UNSCEAR, 2000). By contrast, coral reefs have an opposite habitat of low radioactivity relative to HBRA on the surface of the Earth. As an opposite endmember of HBRA, coral reefs and coral islands may be used as the potential natural laboratory to study the linear or nonlinear relationship between low radiation dose and effects.

Nuclear weapons testing was widely conducted on Bikini Atolls, which were located in the northern Marshall Islands (Robison and Noshkin, 1999). Environmental radiation quality was measured and assessed for resettlement after nuclear weapons testing (Bordner et al., 2016; Buesseler et al., 2018). Although several works focused on radioactivity after nuclear weapons testing (Bordner et al., 2016; Buesseler et al., 2018; Robison and Noshkin, 1999), there are rare historical data on radioactive baseline on Bikini Atolls before nuclear weapon testing.

Similar physical settings occur in the Bikini Atolls and HY atolls with regard to their physical location and chemical component of carbonate sediment. Both the HY and Bikini Atolls are located in the center of the ocean and dominantly composed of calcium carbonate platform, which is mainly manufactured by corals several million years ago (Wang et al., 2018). The latitudes of HY and Bikini Atolls are 15.1°N and 11.5°N, respectively. Our data indicated similar natural radioactivity in all atoll reefs (HY, SJ, BJ, XY, XE, PS, DD, and LH) located in the SCS because of the dominant role of calcium carbonate in sediments (Fig. 6). Additionally, our results were also consistent with previous results on natural radioactivity of coral reefs in the Red Sea (Sam et al., 1998). It was also reported that the activity of ^{40}K in coral reefs was similar between the SCS (9.28 Bq/kg) and Marshall Islands (10.7 ± 0.5 Bq/kg) (Simon et al., 2002). Therefore, the dominant component of calcium carbonate should determine similar natural radioactivity in the HY and Bikini Atolls.

In our study, the absorbed gamma dose rate (D_R) in the HY was 1.16 nGy/h (Table 3), which was lower than the mean D_R (15 nGy/h) on the control island (Majuro Island, capital of the Marshall Islands) and that on other contaminated islands (294 nGy/h on Bikini Island) (Bordner et al., 2016). The control island was also contaminated by close-in fallout because of its location near the sites of nuclear weapons testing relative to the HY in the SCS, thereby resulting in higher D_R on the control island (15 nGy/h) relative to the D_R in the HY atolls (1.16 nGy/h). Therefore, our results may provide invaluable reference for the natural radioactivity before nuclear weapons testing (Fig. 8).

Radioactivity in living coral skeletons and surface marine sediments was simultaneously measured in the fringing reefs and atoll reefs located in the SCS. It displayed a radioactive order of ^{238}U > ^{40}K > ^{228}Ra > ^{226}Ra in coral reefs, which was also different from the order of ^{40}K > ^{238}U = ^{226}Ra > ^{228}Ra in the global soil (UNSCEAR, 2000). We also found similar activities of ^{238}U, ^{226}Ra, and ^{40}K between the marine sediment and the coral skeleton. The similar activities (^{238}U, ^{226}Ra, and ^{40}K) in marine sediments and coral skeletons may give a clue to marine sediments originating from the fragment and weathering of coral skeleton, especially for the atoll reefs far away from the continents. By contrast, high ^{228}Ra activity in coral skeleton relative to marine sediment was observed and resulted in high radioactivity (Ra_{eq}) in coral skeleton due to the decay of short half-life of ^{228}Ra (5.75 a) during the formation of marine sediment. The radioactivity (Ra_{eq}) was higher in the fringing reefs than in the atoll reefs because of the inputs of terrigenous minerals. The unique feature of the abnormally low ^{226}Ra/^{238}U ratio ($k < 0.1$) in coral reefs was observed and attributed to the biological process of active uptake of ^{226}Ra and ^{238}U from seawater by coral polyps rather than the physical process of the ^{238}U-^{230}Th-^{226}Ra decay chain. A comparison of radioactivity in marine sediments along the coastline of China indicated that radioactivity in coral reefs was one order or two orders of magnitude lower than that in other marine environments, the world's average, and China's average. Particularly, the average value of Ra_{eq} in the atoll reefs (4.30 Bq/kg) was < 5% of the world's average (109 Bq/kg). The values of other radiological parameters in coral reefs were also lower than the recommended values. Our results filled the gap of radioactive data on coral skeletons and marine sediments in coral reefs located in the SCS and also provided reference for radiological assessment on Bikini Atolls.

Acknowledgment

The study was financially supported by the National Natural Science Foundation of China (Grant no. 91428203), the Natural Science Foundation of Guangxi Province (2017GXNSFBA198096), Foundation of Key Laboratory of Global Change and Marine-Atmospheric Chemistry (GCMAC1606), the National Key Basic Research Program of China (Grant No. 2013CB956102), and the Bagui Fellowship from Guangxi

Province of China. The entire data can be accessed in the text.

References

Almayahi, B.A., Tajuddin, A.A. and Jaafar, M.S., 2012. Effect of the natural radioactivity concentrations and $^{226}Ra/^{238}U$ disequilibrium on cancer diseases in Penang, Malaysia. Radiat. Prot. Dosim. 81 (10), 1547–1558.

Al-Qaradawi, I., Abdel-Moati, M., Al-Yafei, A.A., Al-Ansari, E., Al-Maslamani, I., Holm, E., Al-Shaikh, I., Mauring, A., Pinto, P.V., Abdulmalik, D., 2015. Radioactivity levels in the marine environment along the Exclusive Economic Zone (EEZ) of Qatar. Mar. Pollut. Bull. 90 (1–2), 323–329.

Baskaran, M., 2012. Dating of biogenic and inorganic carbonates using ^{210}Pb-^{226}Ra disequilibrium method: a review. In: M. Baskaran (Editor), Handbook of Environmental Isotope Geochemistry: vol I. Springer Berlin Heidelberg, Berlin, Heidelberg, pp. 789–809.

Bordner, A.S., Crosswell, D.A., Katz, A.O., Shah, J.T., Zhang, C.R., Nikolic-Hughes, I., Hughes, E.W., Ruderman, M.A., 2016. Measurement of background gamma radiation in the northern Marshall Islands. Proc. Natl. Acad. Sci. U. S. A. 113 (25), 6833–6838.

Buesseler, K.O., Charette, M.A., Pike, S.M., Henderson, P.B., Kipp, L.E., 2018. Lingering radioactivity at the Bikini and Enewetak Atolls. Sci. Total Environ. 621, 1185–1198.

Cho, H.M., Kim, G., 2016. Determining groundwater Ra end-member values for the estimation of the magnitude of submarine groundwater discharge using Ra isotope tracers. Geophys. Res. Lett. 43 (8), 3865–3871.

Cobb, K.M., Charles, C.D., Cheng, H., Kastner, M., Edwards, R.L., 2003. U/Th-dating living and young fossil corals from the central tropical Pacific. Earth Planet. Sci. Lett. 210 (1), 91–103.

Hixon, M.A., Randall, J.E., 2018. Coral reef fishes, Reference Module in Earth Systems and Environmental Sciences. Elsevier.

Hong, G.-H., Hamilton, T., Baskaran, M., Kenna, T., 2011. In: Baskaran, M. (Ed.), Applications of anthropogenic radionuclides as tracers to investigate marine environmental processes. Springer, pp. 367–394.

Hsieh, Y.T. and Henderson, G.M., 2011. Precise measurement of $^{228}Ra/^{226}Ra$ ratios and Ra concentrations in seawater samples by multi-collector ICP mass spectrometry. J. Anal. At. Spectrom. 26 (7), 1338–1346.

Huang, D., Du, J., Deng, B., Zhang, J., 2013. Distribution patterns of particle-reactive radionuclides in sediments off eastern Hainan Island, China: implications for source and transport pathways. Cont. Shelf Res. 57, 10–17.

Huang, Y., Lu, X., Ding, X., Feng, T., 2015. Natural radioactivity level in beach sand along the coast of Xiamen Island, China. Mar. Pollut. Bull. 91 (1), 357–361.

IAEA, 2005. Worldwide Marine Radioactivity Studies (WOMARS): Radionuclide Levels in Oceans and Seas. IAEA, Vienna.

Johansen, M.P., Ruedig, E., Tagami, K., Uchida, S., Higley, K., Beresford, N., 2015. Radiological dose rates to marine fish from the Fukushima Daiichi accident: the first three years across the North Pacific. Environ. Sci. Technol. 49 (3), 1277–1285.

Koide, M., Bruland, K.W., Goldberg, E.D., 1973. Th-228/Th-232 and Pb-210 geochronologies in marine and lake sediments. Geochim. Cosmochim. Acta 37 (5), 1171–1187.

LaBrecque, J.J., Cordoves, P.R., Cordoves, M.A., Perez, K., Palacios, D. and Alfonso, J.A., 2010. Distribution of ^{137}Cs, ^{40}K, ^{232}Th and ^{238}U in coastal marine sediments of Margarita Island, Venezuela. J. Radioanal. Nucl. Chem. 283 (3), 669–674.

Lin, W., Chen, L., Yu, W., Ma, H., Zeng, Z., Lin, J., Zeng, S., 2015a. Radioactivity impacts of the Fukushima Nuclear Accident on the atmosphere. Atmos. Environ. 102, 311–322.

Lin, W.H., Chen, L.Q., Jian-Hua, H.E., Hao, M.A., Zeng, Z., Zeng, S., 2015b. Review on monitoring marine radioactivity since the Fukushima Nuclear Accident. Chin. Environ. Sci. 35 (1), 269–276.

Lin, W., Chen, L., Yu, W., Ma, H., Zeng, Z., Zeng, S., 2016a. Radioactive source-term of the Fukushima Nuclear Accident. Sci. China: Earth Sci. 59 (1), 214–222.

Lin, W., Chen, L., Zeng, S., Li, T., Wang, Y. and Yu, K., 2016b. Residual β activity of particulate ^{234}Th as a novel proxy for tracking sediment resuspension in the ocean. Sci. Rep. 6, 27069.

Lin, W., Yu, K., Wang, Y., Fan, T., Mo, M., 2018a. Combination of field-based natural gamma radiation and laboratory-based HPGe gamma spectrometry to investigate the natural radionuclides of a long coral core (928 m) in the South China Sea. Acta Geol. Sin. (Engl. Ed.) 92 (Supp 2), 80–83.

Lin, W., Yu, K., Wang, Y., Liu, X., Wang, J., Ning, Q., Li, Y., 2018b. Extremely low radioactivity in marine sediment of coral reefs and its mechanism. Chin. Sci. Bull. 63 (21), 2173–2183.

Lindahl, P., Asami, R., Iryu, Y., Worsfold, P., Keith-Roach, M., Choi, M.-S., 2011. Sources of plutonium to the tropical Northwest Pacific Ocean (1943–1999) identified using a natural coral archive. Geochim. Cosmochim. Acta 75 (5), 1346–1356.

Liu, X., Lin, W., 2018. Natural radioactivity in the beach sand and soil along the coastline of Guangxi Province, China. Mar. Pollut. Bull. 135, 446–450.

McCulloch, M., Fallon, S., Wyndham, T., Hendy, E., Lough, J., Barnes, D., 2003. Coral record of increased sediment flux to the inner Great Barrier Reef since European settlement. Nature 421 (6924), 727–730.

Moberg, F., Folke, C., 1999. Ecological goods and services of coral reef ecosystems. Ecol. Econ. 29 (2), 215–233.

Moore, W.S., 2010. The effect of submarine groundwater discharge on the ocean. Annu. Rev. Mar. Sci. 2 (2), 59–88.

Moore, W.S. and Krishnaswami, S., 1972. Coral growth rates using ^{228}Ra and ^{210}Pb. Earth Planet. Sci. Lett. 15 (2), 187–190.

Nozaki, Y., Yamamoto, Y., 2001. Radium-228 based nitrate fluxes in the eastern Indian Ocean and the South China Sea and a silicon-induced "alkalinity pump" hypothesis. Glob. Biogeochem. Cycles 15 (3), 555–567.

Ojovan, M.I., Lee, W.E., 2014. In: Ojovan, M.I., Lee, W.E. (Eds.), Naturally occurring radionuclides - an introduction to nuclear waste immobilisation. Elsevier, pp. 31–39.

Pan, C.-G., Yu, K.-F., Wang, Y.-H., Zhang, R.-J., Huang, X.-Y., Wei, C.-S., Wang, W.-Q., Zeng, W.-B., Qin, Z.-J., 2018. Species-specific profiles and risk assessment of perfluoroalkyl substances in coral reef fishes from the South China Sea. Chemosphere 191, 450–457.

Patiris, D.L., Tsabaris, C., Anagnostou, C.L., Androulakaki, E.G., Pappa, F.K., Eleftheriou, G., Sgouros, G., 2016. Activity concentration and spatial distribution of radionuclides in marine sediments close to the estuary of Shatt al-Arab/Arvand Rud River, the Gulf. J. Environ. Radioact. 157, 1–15.

Pham, M.K., Sanchezcabeza, J.A., Povinec, P.P., Andor, K., Arnold, D., Benmansour, M., Bikit, I., Carvalho, F.P., Dimitrova, K., Edrev, Z.H., 2008. A new Certified Reference Material for radionuclides in Irish sea sediment (IAEA-385). Appl. Radiat. Isot. 66 (11), 1711–1717.

Ravisankar, R., Chandramohan, J., Chandrasekaran, A., Jebakumar, J.P.P., Vijayalakshmi, I., Vijayagopal, P., Venkatraman, B., 2015. Assessments of radioactivity concentration of natural radionuclides and radiological hazard indices in sediment samples from the East coast of Tamilnadu, India with statistical approach. Mar. Pollut. Bull. 97 (1–2), 419–430.

Robison, W.L., Noshkin, V.E., 1999. Radionuclide characterization and associated dose from long-lived radionuclides in close-in fallout delivered to the marine environment at Bikini and Enewetak Atolls. Sci. Total Environ. 237-238, 311–327.

Sabatier, P., Reyss, J.-L., Hall-Spencer, J.M., Colin, C., Frank, N., Tisnerat-Laborde, N., Bordier, L. and Douville, E., 2012. ^{210}Pb-^{226}Ra chronology reveals rapid growth rate of Madrepora oculata and Lophelia pertusa on world's largest cold-water coral reef. Biogeosciences 9 (3), 1253–1265.

Saha, N., Webb, G.E., Zhao, J.-X., 2016. Coral skeletal geochemistry as a monitor of inshore water quality. Sci. Total Environ. 566, 652–684.

Sam, A.K., Ahamed, M.M.O., Khangi, F.A.E., El Nigumi, Y.O., Holm, E., 1998. Radioactivity levels in the Red Sea coastal environment of Sudan. Mar. Pollut. Bull. 36 (1), 19–26.

Shuaibu, H.K., Khandaker, M.U., Alrefae, T., Bradley, D.A., 2017. Assessment of natural radioactivity and gamma-ray dose in monazite rich black Sand Beach of Penang Island, Malaysia. Mar. Pollut. Bull. 119 (1), 423–428.

Simon, S., Graham, J. and Terp, S., 2002. Uptake of ^{40}K and ^{137}Cs in native plants of the Marshall Islands. J. Environ. Radioact. 59 (2), 223–243.

Stewart, G.M., Fowler, S.W., Fisher, N.S., 2008. The bioaccumulation of U- and Th-series radionuclides in marine organisms. In: Krishnaswami, S., Cochran, J.K. (Eds.), U-Th Series Nuclides in Aquatic Systems. Elsevier, 269–305.

Trevisi, R., Risica, S., D'Alessandro, M., Paradiso, D., Nuccetelli, C., 2012. Natural radioactivity in building materials in the European Union: a database and an estimate of radiological significance. J. Environ. Radioact. 105, 11–20.

Uddin, S., Behbehani, M., 2018. Concentrations of selected radionuclides and their spatial distribution in marine sediments from the northwestern Gulf, Kuwait. Mar. Pollut. Bull. 127, 73–81.

UNSCEAR, 2000. Sources, effects of ionizing radiation. In: UNSCEAR (Ed.), Report to the General Assembly With Annex B. United Nations, New York.

Valan, I.I., Maniyarasan, S., Mathiyarasu, R., Sridhar, S.G.D., Narayanan, V., Stephen, A., 2016. Seasonal observation on radionuclide concentration in Krusadai Island Mangroves, Gulf of Mannar, India. J. Radioanal. Nucl. Chem. 310 (3), 1277–1288.

Van Schmus, W.R., 1995. Natural radioactivity of the crust and mantle. Global Earth Phys 59 (20), 4285–4298.

Veron, J.E.N., Devantier, L.M., Turak, E., Green, A.L., Kininmonth, S., Stafford-Smith, M., Peterson, N., 2011. The coral triangle. In: Dubinsky, Z., Stambler, N. (Eds.), Coral Reefs: An Ecosystem in Transition. Springer, Netherlands, pp. 47–55.

Wang, Z., 2002. Natural radiation environment in China. Int. Congr. Ser. 1225 (01), 39–46.

Wang, X., Du, J., 2016. Submarine groundwater discharge into typical tropical lagoons: a case study in eastern Hainan Island, China. Geochem. Geophys. Geosyst. 17 (11), 4366–4382.

Wang, Q., Song, J., Li, X., Yuan, H., Li, N., Cao, L., 2015. Environmental radionuclides in a coastal wetland of the Southern Laizhou Bay, China. Mar. Pollut. Bull. 97 (1–2), 506–511.

Wang, J., Du, J., Bi, Q., 2017a. Natural radioactivity assessment of surface sediments in the Yangtze Estuary. Mar. Pollut. Bull. 114 (1), 602–608.

Wang, L., Ma, Z., Sun, Z., Wang, Y., Wang, X., Cheng, H. and Xiao, J., 2017b. U concentration and $^{234}U/^{238}U$ of seawater from the Okinawa Trough and Indian Ocean using MC-ICPMS with SEM protocols. Mar. Chem. 196 (Supplement C), 71–80.

Wang, R., Yu, K., Jones, B., Wang, Y., Zhao, J., Feng, Y., Bian, L., Xu, S., Fan, T., Jiang, W., Zhang, Y., 2018. Evolution and development of Miocene "island dolostones" on Xisha Islands, South China Sea. Mar. Geol. 406, 142–158.

Waters, C.N., Zalasiewicz, J., Summerhayes, C., Barnosky, A.D., Poirier, C., Gałuszka, A., Cearreta, A., Edgeworth, M., Ellis, E.C., Ellis, M., Jeandel, C., Reinhold, 11, J.R.M., Richter, D.D., Steffen, W., Syvitski, J., Vidas, D., Wagreich, M., Williams, M., Zhisheng, A., Grinevald, J., Odada, E., Oreskes, N., Wolfe, A.P., 2016. The Anthropocene is functionally and stratigraphically distinct from the Holocene. Science 351 (6269), 1–10.

Xia, Z., Jia, P., Ma, S., Liang, K., Shi, Y., Waniek, J.J., 2013. Sedimentation in the Lingdingyang Bay, Pearl River Estuary, Southern China. J. Coastal Res. 66, 12–24.

Xu, L., Liu, X., Sun, L., Yan, H., Liu, Y., Luo, Y., Huang, J., Wang, Y., 2010. Distribution of radionuclides in the guano sediments of Xisha Islands, South China Sea and its implication. J. Environ. Radioact. 101 (5), 362–368.

Xu, L.-Q., Liu, X.-D., Sun, L.-G., Yan, H., Liu, Y., Luo, Y.-H., Huang, J., 2011. Geochemical evidence for the development of coral island ecosystem in the Xisha Archipelago of South China Sea from four ornithogenic sediment profiles. Chem. Geol. 286 (3), 135–145.

Yu, K.N., Guan, Z.J., Stokes, M.J., Young, E.C.M., 1994. Natural and artificial radionuclides in seabed sediments of Hong Kong. Nuclear Geophys 8, 45–48.
Yu, K.F., Zhao, J.X., Shi, Q., Meng, Q.S., 2009. Reconstruction of storm/tsunami records over the last 4000 years using transported coral blocks and lagoon sediments in the southern South China Sea. Quat. Int. 195 (1), 128–137.
Yu, K., Hua, Q., Zhao, J.X., Hodge, E., Fink, D. and Barbetti, M., 2010. Holocene marine ^{14}C reservoir age variability: evidence from ^{230}Th-dated corals in the South China Sea. Paleoceanogr. 25, 375–387.
Zhang, R., Zhang, R., Yu, K., Wang, Y., Huang, X., Pei, J., Wei, C., Pan, Z., Qin, Z., Zhang, G., 2018. Occurrence, sources and transport of antibiotics in the surface water of coral reef regions in the South China Sea: potential risk to coral growth. Environ. Pollut. 232, 450–457.
Zhao, M., Yu, K., Shi, Q., Zhang, Q., Yan, H., Huang, L., 2013. Source, distribution and influencing factors of sediments on Luhuitou fringing reef, Northern South China Sea. Chin. Sci. Bull. 58 (17), 1583–1589.
Zhao, F., Wu, M., Zhou, P., Li, D., Zhao, L., Zheng, Y., Cai, W., Fang, H., Huang, C., 2015. Radionuclides in surface sediments from the Huangmaohai Estuary-Guanghai Bay and its adjacent sea area of the South China Sea. J. Trop. Oceanogr. 34 (4), 77–82.
Zhou, P., Li, D., Li, H., Fang, H., Huang, C., Zhang, Y., Zhang, H., Li, Z., Zhou, J., Wang, H., 2015. Distribution of radionuclides in a marine sediment core off the waterspout of the nuclear power plants in Daya Bay, northeastern South China Sea. J. Environ. Radioact. 145, 102–112.